Dynamic Response of Geomaterials Considering Thermal Stress and Its Application in Seismic Engineering

Fengyan Qin[1], Fulian Yang[1]*, Qingyun Ge[1], Jing Zheng[1,2]

[1]School of Architecture and Civil Engineering, West Anhui University, Liu'an 237012, China
[2]Green Building and Intelligent Construction Technology Research Center, West Anhui University, Liu'an 237012, China

Corresponding Author Email: 05000069@wxc.edu.cn

ABSTRACT

With the ongoing challenges of global climate change and the rapid development of underground engineering, the mechanical behavior of geomaterials under the combined effects of thermal stress and dynamic loading has become a research focus. Underground structures, such as tunnels and foundation pits, often encounter complex stress environments, especially under extreme dynamic loads like earthquakes, where temperature-induced thermal stress may significantly alter the performance of geomaterials. Although previous studies have examined the dynamic response of geomaterials, most methods have primarily focused on the effects of single stresses, with limited attention to the coupling effects of thermal stress and dynamic loads, leading to insufficient predictive accuracy. To address this issue, this paper first selects and establishes a heat transfer model for the dynamic thermal response of geomaterials and systematically explores the stress-strain evolution laws of geomaterials under compound stress conditions, with particular emphasis on the analysis of thermal stress in seismic engineering. This research provides a theoretical basis for optimizing underground structure design and enhancing seismic performance.

1. INTRODUCTION

In recent years, with the increasing global climate warming and the growing construction of underground engineering, the mechanical behavior of geomaterials under the action of thermal stress and dynamic loads has received widespread attention [1-3]. In practical engineering such as underground tunnels, deep foundation pits, geothermal energy development, and other projects, geomaterials are often exposed to complex stress environments, especially under extreme dynamic loads such as earthquakes, where the superimposed effects of temperature-induced thermal stress and seismic loads may lead to significant changes in the performance of geomaterials [4, 5]. Therefore, an in-depth study of the dynamic response of geomaterials considering thermal stress is of great engineering significance for improving the safety and stability of underground structures.

Research on the behavior of geomaterials under the coupled effects of thermal and dynamic loads has important theoretical and practical value. First, understanding the stress-strain relationship of geomaterials under compound stress conditions helps optimize the design of underground structures, reducing the risk of damage caused by temperature and load [6-10]. Second, by establishing accurate dynamic thermal response models, the impact of natural disasters such as earthquakes on underground structures can be better predicted and mitigated [11, 12]. Therefore, conducting research in this area not only promotes the further development of geomechanics theory but

also provides effective support for disaster prevention and mitigation in seismic engineering.

However, existing research methods mostly focus on single stress effects, such as pure dynamic analysis or pure thermal stress analysis, with limited consideration of the dynamic response of geomaterials under the coupled action of thermal stress and dynamic loads [13-15]. Even in some studies involving compound stress conditions, the thermal stress effects induced by temperature changes are often neglected, or the model selection and calculation processes are overly simplified, making it difficult to accurately reflect the mechanical behavior of geomaterials under complex working conditions [16-20]. The limitations of these studies lead to uncertainties in predicting the response of geomaterials under compound stress conditions in practical engineering applications, which urgently require improvement and further research.

In response to the above issues, this paper mainly conducts research in two aspects. First, for the dynamic thermal response of geomaterials, a reasonable heat transfer model is selected and established to provide a theoretical basis for simulating the behavior of geomaterials under the combined action of thermal stress and dynamic loads. Second, this paper conducts an in-depth analysis of the thermal stress of geomaterials under compound stress conditions in seismic engineering, systematically exploring the stress-strain evolution laws of geomaterials under the coupling of temperature and dynamic effects. These studies not only

provide new insights for the analysis of the dynamic response of geomaterials but also provide theoretical support for improving the seismic performance and design rationality of underground structures, with significant academic value and engineering application prospects.

2. SELECTION AND ESTABLISHMENT OF HEAT TRANSFER MODEL FOR DYNAMIC THERMAL RESPONSE OF GEOMATERIALS

In the process of studying the thermal dynamic response of geomaterials, obtaining the thermal physical parameters of geomaterials and selecting an appropriate heat transfer model are key to conducting accurate analysis. The mechanical behavior of geomaterials under complex working conditions is influenced not only by external dynamic loads but also by thermal stress caused by temperature changes. Therefore, the study of their thermal dynamic response requires consideration of the coupling effects of temperature and mechanical factors simultaneously. The thermal physical parameters of geomaterials include thermal conductivity, specific heat capacity, and thermal diffusivity, which directly influence the conduction and distribution of temperature within geomaterials and determine the response speed and intensity of geomaterials under the influence of external heat sources and dynamic loads. Therefore, accurately measuring these parameters is crucial for constructing a reliable thermal dynamic response model. Figure 1 shows the schematic diagram of the dynamic thermal response test system for geomaterials.

Based on these thermal physical parameters, the selection and establishment of a heat transfer model is also a core part of thermal dynamic response analysis. In the thermal dynamic coupling analysis of geomaterials, a reasonable heat transfer model can effectively simulate the changes in the internal temperature field and stress field of geomaterials. Common heat transfer models, such as Fourier's heat conduction model, can be used to describe the diffusion process of heat in geomaterials, while coupling models combined with dynamic analysis can further consider the superimposed effects of dynamic loads, such as earthquakes, and thermal stress. In practical applications, the selection of the model needs to fully consider the actual working conditions and material properties of geomaterials to ensure accurate prediction of the stress-strain behavior of geomaterials under thermal dynamic coupling conditions.

Analytical methods, due to their simplicity and wide applicability, have become the mainstream methods for studying the thermal physical parameters of geomaterials. By substituting the necessary parameters into classical formulas, such as the cylindrical source model, line heat source model, or semi-infinite slab heat conduction model, the thermal physical parameters of soil, such as thermal conductivity, can be quickly obtained. However, these methods may have certain limitations when applied to complex ground source heat pump systems. For example, although the cylindrical source model can simulate the actual working conditions of underground U-shaped heat exchangers to some extent, its simplified treatment leads to significant calculation errors, especially when facing thermal dynamic response analysis, where these errors may affect the accuracy of the results.
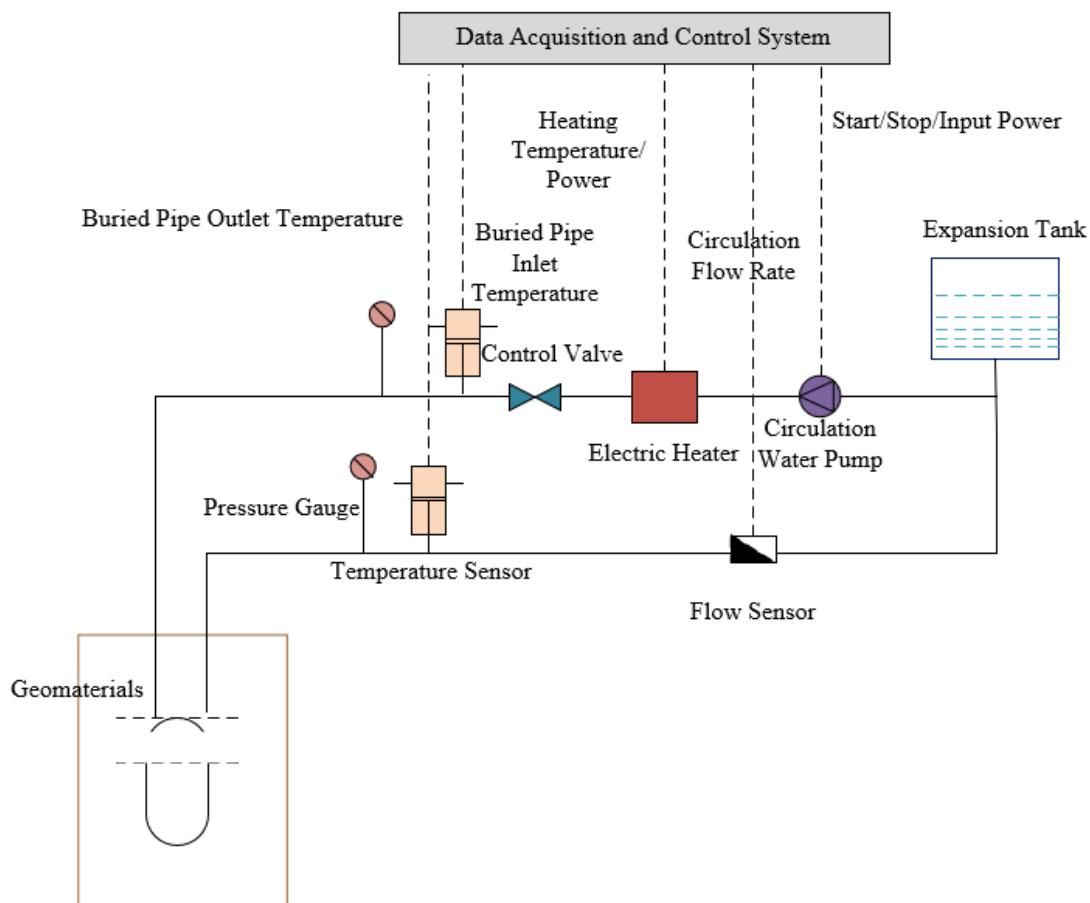

Figure 1. Schematic diagram of the dynamic thermal response test system for geomaterials

In contrast, numerical methods offer greater flexibility and accuracy, especially suitable for complex thermal-dynamic coupling problems. In the analysis of the thermal dynamic response of geomaterials, numerical methods discretize the calculation region using the finite element method, dividing the geomaterials into multiple computational units and solving these units using differential equations. This method can consider the complex thermal conduction and mechanical interactions within geomaterials, especially under dynamic loads, where numerical methods can more accurately simulate the thermal-mechanical response of geomaterials. However, this method is more cumbersome in the calculation process and requires a higher level of technical expertise and computational resources.

In seismic engineering, temperature changes are often accompanied by the superimposed effects of dynamic loads, which make the internal stress state of geomaterials more complex. This paper selects the line heat source model for analyzing the thermal dynamic response of geomaterials to provide effective theoretical support. The basic principle of the line heat source model lies in treating the buried pipe heat exchanger as an idealized linear heat source and calculating the thermal physical parameters of geomaterials by analyzing its heat exchange process with the surrounding soil, thereby providing fundamental data for subsequent thermal dynamic response analysis. This model can accurately simulate the local thermal conduction characteristics of the heat source to the surrounding soil, which is crucial for understanding the thermal-mechanical coupling behavior of geomaterials under dynamic loads. By neglecting factors such as axial heat transfer of the U-tube, contact thermal resistance, and atmospheric temperature and groundwater migration, the line heat source model simplifies the complex thermal-mechanical coupling process, making the calculation more intuitive and adaptable to various scenarios in practical engineering applications.

According to the assumptions of the line heat source model, the heat exchange process within the borehole is approximated as a steady-state heat transfer process. This is because the circulating medium within the pipe has a small volumetric heat capacity and a high thermal conductivity, making the temperature difference between the circulating medium and the pipe wall negligible. The heat exchange process is primarily controlled by the unsteady heat transfer process between the exterior of the borehole and the surrounding infinite soil medium. In the unsteady heat transfer process, the initial temperature of the soil is considered uniform and constant, and the temperature distribution after heating changes with time and spatial position. Below, this paper further elaborates on the model's principle from three aspects: heat transfer within the borehole, heat transfer outside the borehole, and the fitting process.

(1) Heat transfer within the borehole. Heat transfer within the borehole is the first step in the line heat source model. In this step, it is assumed that the temperature of the circulating medium in the U-tube heat exchanger is the same as that of the pipe wall. Due to the small volumetric heat capacity and high thermal conductivity of the circulating medium, this assumption is valid. This means that the thermal resistance and thermal capacity within the circulating medium can be neglected, simplifying the calculation process. Since the contact between the pipe wall and the backfill material, as well as between the backfill material and the surrounding soil, is very tight, contact thermal resistance is also neglected. These

simplifications allow the heat transfer process within the borehole to be approximated as a steady-state heat transfer process, laying the foundation for subsequent analysis. Assuming that the average water temperature in the supply and return pipes is denoted by S_d, for the thermal response analysis experiment, this is the average of the inlet and outlet water temperatures. The wall temperature of the borehole is denoted by S_y, and the heat flux density of the medium in the pipe is denoted by w. According to the classical steady-state heat conduction equation, we have:

$$S_d - S_y = wE_p \tag{1}$$

The value of w in the thermal response experiment can be obtained by calculating the heating power, with the formula $w=W/G$. $G=lz_o(s_{IN}-s_{OUT})$, where G represents the depth of the borehole. The total thermal resistance within the borehole is denoted by E_p. Assuming that the convective heat transfer resistance between the medium in the pipe and the inner wall of the U-tube is denoted by E_d, the thermal resistance of the U-tube wall is denoted by E_o, the thermal resistance of the backfill material in the borehole is denoted by E_y, the inner diameter of the U-tube is denoted by f_u, the convective heat transfer coefficient between the medium in the pipe and the inner wall of the U-tube is denoted by g, the thermal conductivity of the U-tube is denoted by η_o, the equivalent diameter of the U-tube is denoted by f_{rp}, the inner diameter of the equivalent pipe is denoted by f_{ru}, whose value is f_{rp}-$(f_p$-$f_u)$, the outer diameter of the U-tube is denoted by f_p, the thermal conductivity of the backfill material is denoted by η_y, the diameter of the borehole is denoted by f_y, and the convective heat transfer coefficient within the pipe is denoted by g. Thus, we have the formula:

$$E_P = E_d + E_o + E_y$$
$$= \frac{1}{2\pi f_u g} + \frac{1}{4\pi\eta_o}\ln\left(\frac{f_{rp}}{f_{ru}}\right) + \frac{1}{4\pi\eta_y}\ln\left(\frac{f_y}{f_r}\right) \tag{2}$$

Assuming that the thermal conductivity of the heat transfer medium in the buried pipe is denoted by η, and the Nusselt number of the medium at the average temperature at a certain time is denoted by Vi. When the flow state of the medium is turbulent and the inner wall is smooth, the formula for calculating g is as follows:

$$g = Vi\frac{\eta}{f_{ru}}0 \tag{3}$$

(2) Heat transfer outside the borehole is the second key step of the model. Here, the focus is on the heat exchange process between the exterior of the borehole and the surrounding infinite soil medium. Since the soil outside the borehole is considered homogeneous and initially at a constant temperature, as the operating time of the heat exchanger increases, the soil temperature gradually rises, exhibiting the characteristics of unsteady heat transfer. In the line heat source model, the thermal conduction process of the soil is regarded as the diffusion of heat from the idealized linear heat source to the surrounding soil medium. The simulation of this process is crucial for analyzing the stress and deformation response of geomaterials under temperature changes, especially under dynamic loads such as earthquakes, where this thermal

conduction process may lead to the concentration of thermal stress, thereby affecting the mechanical properties of geomaterials. Assuming that the average thermal conductivity of the soil is denoted by η_t, the average density of the soil is denoted by ϑ_t, the average specific heat capacity of the soil is denoted by z_t, the temperature of the soil surrounding the borehole is denoted by S, the heat exchange time is denoted by λ, and the original geothermal temperature of the soil is denoted by S_{dd}, the mathematical description of the heat transfer for this model can be expressed as follows:

$$
\begin{aligned}
\frac{\eta_t}{\vartheta_t z_t}\left(\frac{\partial^2 S}{\partial e^2}+\frac{1}{e}\frac{\partial S}{\partial e}\right)=\frac{\partial S}{\partial \lambda} &\qquad \frac{f_y}{2}\leq e<\infty, \lambda>0 \\
S=S_{dd} &\qquad \frac{f_y}{2}\leq e<\infty, \lambda=0 \\
w=-\eta_t\left.\frac{\partial S}{\partial e}\right|_{e=\frac{f_y}{2}} &\qquad \lambda>0 \\
S=S_{dd} &\qquad \lambda>0, e\leftarrow\infty
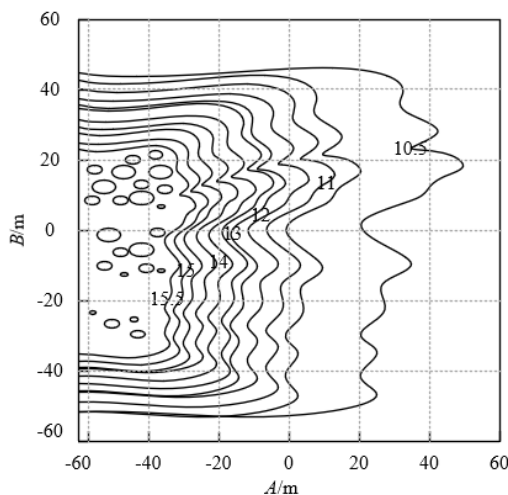\end{aligned}
\qquad (4)
$$

Based on the above formula, the soil temperature distribution corresponding to time λ can be obtained, but the calculation process is rather complex. Assuming the exponential integral is represented by $Ru(a)=\int_a^\infty e^{-t}/t\, dt$, when time tends to infinity, this integral can be expressed as $Ru(a)=ln(1/a)-\varepsilon$, where ε denotes the Euler constant. The simplified formula is given as follows:

$$
S_y = S_{dd} + \frac{w}{4\pi\eta_t}\bullet Ru\left(\frac{f_y^2\vartheta_t z_t}{16\eta_t\lambda}\right)
\qquad (5)
$$

Furthermore, the thermal resistance outside the borehole can be obtained by the following formula:

$$
E_q = \frac{1}{4\pi\eta_t}\bullet Ru\left(\frac{f_y^2\vartheta_t z_t}{16\eta_t\lambda}\right)
\qquad (6)
$$

(3) In the analysis of the thermal dynamic response of geomaterials, the fitting process involves comparing the model calculation results with experimental data to calibrate the model parameters. Specifically, the soil thermal conductivity and other thermal physical parameters are set through parameter estimation methods, and the fluid average temperature output from the calculation program is compared with the actual experimental measurements. Figure 2 shows the temperature field distribution at the end of diffusion with a flow direction of 0°. By using the Gaussian minimization method, the sum of the squared differences between the calculated and experimental values is minimized, thereby optimizing the model's accuracy. This fitting process is a key step in ensuring the reliability and precision of the line heat source model in practical seismic engineering applications. By combining Eqs. (1) and (2), the comprehensive heat transfer equation between the medium in the underground buried pipe and the underground geomaterials can be obtained, which is:

$$
S_d = S_{dd} + w\left(E_P + \frac{1}{4\pi\eta_t}\bullet\left(\ln\left(\frac{16\eta_t\lambda}{f_y^2\vartheta_t z_t}\right)-\varepsilon\right)\right)
\qquad (7)
$$

If the average temperature of the supply and return water and the logarithm of time are taken as the vertical and horizontal coordinates, respectively, the above equation can be rearranged as:

$$
\begin{aligned}
S_d = &\frac{w}{4\pi\eta_t}\ln\lambda + S_{dd} + \\
&w\left(E_P + \frac{1}{4\pi\eta_t}\bullet\left(\ln\left(\frac{16\eta_t}{f_y^2\vartheta_t z_t}\right)-\varepsilon\right)\right)
\end{aligned}
\qquad (8)
$$

The equivalent expression of the above equation is $y=lx+\tau$. For the thermal response experiment, the most important parameter required is the average thermal conductivity of the geomaterials, which is characterized by the slope of $y=lx+\tau$. To obtain the slope of $y=lx+\tau$, the experimental data must be fitted based on the least squares method, ensuring that the sum of the squared differences between the fitted Y value (the calculated fitted average temperature value) and the actual given Y value (the actual average temperature value of the supply and return water at time λ) is minimized. The specific calculation formula is as follows:

$$
l = \frac{\sum a_u b_u - v\overline{a}\overline{b}}{\sum a_u^2 - v\overline{a}^2} \qquad y = \overline{b} - l\overline{a}
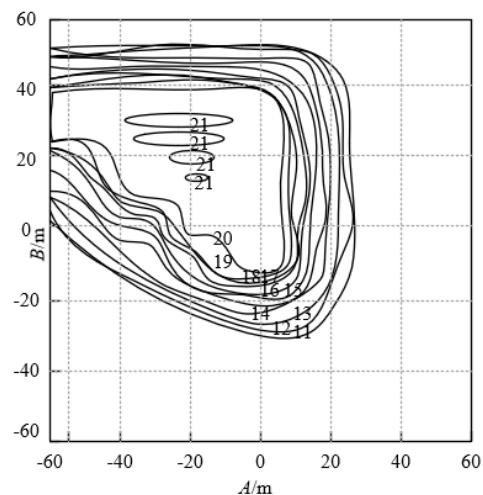\qquad (9)
$$

Figure 2. Temperature field distribution at the end of diffusion with a flow direction of 0°

At this point, the thermal physical parameters of the geomaterials can be calculated. Furthermore, finite element methods or other numerical simulation techniques can be used to dynamically simulate the constructed thermal-mechanical coupling model. By applying time-varying stress fields representing dynamic loads such as earthquakes, the stress distribution, deformation patterns, and potential failure modes of geomaterials under the combined effects of temperature changes and dynamic loads can be studied.

3. THERMAL STRESS ANALYSIS OF GEOMATERIALS UNDER COMPOUND STRESS CONDITIONS IN SEISMIC ENGINEERING

In seismic engineering, this paper introduces the equivalent linearization analysis method to analyze the thermal stress of geomaterials under compound stress conditions, aiming to understand and predict the mechanical behavior of geomaterials under thermal-dynamic coupling. In this method, it is necessary to reasonably define and evaluate the "compound thermal shear strain" under compound stress conditions to ensure that the influence of thermal stress and thermal strain on the dynamic response of geomaterials can be accurately simulated. Figure 3 shows the soil profile and measurement point layout of the thermal stress experimental site in seismic engineering.

Considering the complexity of thermal stress, especially under the combined action of seismic loads and temperature changes, the internal geomaterials often exhibit a compound stress state. In such cases, relying solely on traditional shear strain criteria may not be sufficient to reflect the true deformation behavior of geomaterials under the combined action of vertical seismic motion and thermal stress. Therefore, it is particularly important to use compound shear strain to describe the thermal stress response of geomaterials. The compound shear strain here includes octahedral shear strain, generalized shear strain, pure shear strain, symbolic shear strain, and deviatoric shear strain.

For this purpose, the thermal stress analysis of geomaterials in seismic engineering should follow the following principles: 1) Under pure shear stress conditions, the compound thermal shear strain should be equal to the known thermal shear strain to meet the requirements of equivalent linearization in horizontally layered sites under thermal conditions. This means that, under thermal dynamic conditions, the shear wave propagation process in geomaterials needs to accurately capture the stress distribution changes caused by temperature gradients. 2) Under the action of vertical seismic motion alone, the compound thermal shear strain should be slightly greater than the vertical thermal strain. This principle is consistent with the principles of geotechnical experiments, ensuring that the changes in the vertical confined compression modulus of geomaterials under the combined effects of temperature changes and seismic loads can be reasonably reflected. Particularly in dynamic triaxial tests, the relationship between damping ratio and thermal shear strain can be directly used to adjust the modulus ratio in thermal stress analysis, thereby improving the accuracy of the analysis. Assuming that the second invariant of the deviatoric strain tensor is denoted by K'_2, considering the above-mentioned types of compound shear strain, only pure shear strain ε_t meets the condition:

$$\varepsilon_t = \Gamma = 2\sqrt{K'_2} = \sqrt{\frac{2}{3}\left[(\gamma_1 - \gamma_2)^2 + (\gamma_2 - \gamma_3)^2 + (\gamma_3 - \gamma_2)^2\right]} \quad (10)$$

$$= \sqrt{\frac{2}{3}\left[(\gamma_a - \gamma_b)^2 + (\gamma_b - \gamma_c)^2 + (\gamma_c - \gamma_a)^2 + \frac{2}{3}\left(\varepsilon_{ab}^2 + \varepsilon_{bc}^2 + \varepsilon_{ca}^2\right)\right]}$$

$$= \sqrt{3}\bar{\varepsilon} = \sqrt{\frac{3}{2}}\varepsilon_{oct} = \frac{1}{\sqrt{2}}\varepsilon_{\delta} = \sqrt{2}\bar{\varepsilon}'$$

For plane strain problems, $\varepsilon_{ca}=\varepsilon_{cb}=\gamma_c=0$. The above equation becomes:

$$\varepsilon_t = \sqrt{\frac{2}{3}(\gamma_a - \gamma_b)^2 + \frac{2}{3}(\gamma_a^2 - \gamma_b^2)^2 + \varepsilon_{ab}^2} \quad (11)$$

In seismic engineering, the equivalent linearization analysis method is primarily used to handle the complex stress-strain relationships of geomaterials under seismic loads and temperature changes. Therefore, the setting of convergence criteria is key to ensuring the accuracy of the analysis results. In equivalent linearization analysis, convergence is typically judged by the criterion that the difference in equivalent thermal shear strain between two consecutive iterations is small, with the change being less than a certain allowable value, or by reaching a predetermined maximum number of iterations. This means that during multiple iterations, it is necessary to ensure that the equivalent thermal shear strain gradually stabilizes after each iteration to reflect the actual response of geomaterials under compound stress conditions. Let $\varepsilon_{ME,v+1}$ and $\gamma_{ME,v}$ be the average shear strain values of the $v+1$-th and v-th iterations, respectively, then:

$$\left|\frac{\varepsilon_{ME,v+1} - \varepsilon_{ME,v}}{\varepsilon_{ME,v}}\right| \leq (1\% \sim 5\%) \quad (12)$$

Assuming that the dynamic displacement in the a or b direction of node v in the u-th iteration cycle is denoted by x^u_v, the maximum value selected in the dynamic analysis of the u-th iteration cycle is denoted by MAX ( ). The number of nodes in the element is denoted by v_o. The maximum standard displacement value X^u_{MAX} can also be used as a criterion, then:

$$X^u_{MAX} = MAX\left(\sqrt{\sum_{v=1}^{v_o}\left(x^u_v\right)^2 \Big/ v_o}\right) \quad (13)$$

$$\sigma X_{MAX} = \frac{\left|X^{u+1}_{MAX} - X^u_{MAX}\right|}{X^u_{MAX}} \leq (1\% \sim 5\%) \quad (14)$$

The convergence requirements of each element are the guarantee for achieving global analysis accuracy. In this analysis process, all computational elements must meet the convergence criteria, even those that initially met the convergence conditions must be recalculated for convergence in subsequent iterations. This requirement ensures the consistency of the overall computation, avoiding local areas from affecting the overall analysis results due to not meeting accuracy requirements. Additionally, since strictly achieving the equivalence of shear stiffness and damping ratio for all elements in practice is extremely difficult, it is generally emphasized that the equivalence of shear modulus is strictly enforced, while the damping ratio is handled by weighted averaging across all elements. This approach allows for simplifying the computation process to some extent while maintaining a high level of result accuracy.
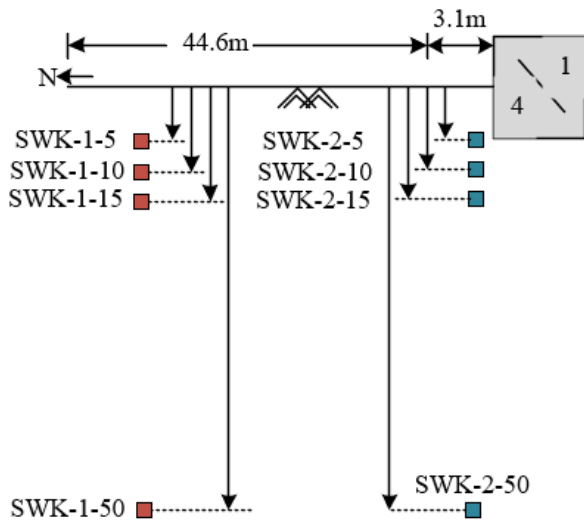
Figure 3. Soil profile and measurement point layout of the thermal stress experimental site in seismic engineering
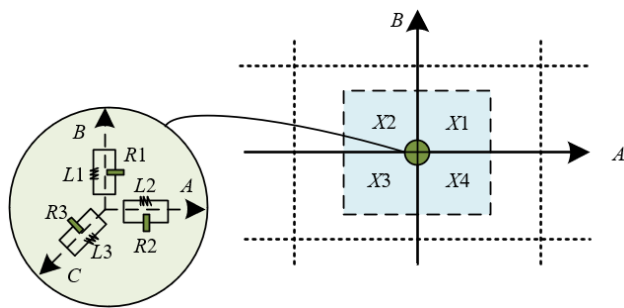

Figure 4. Schematic diagram of artificial boundaries

To further improve the analysis accuracy, the analysis of compound thermal shear strain is usually conducted under the assumption that Poisson's ratio remains unchanged, and the strain values at the center of the elements are used for calculation. Meanwhile, the setting of artificial boundaries should be done far from the discrete source to ensure that the elements in the boundary area do not affect the equivalent linearization process, thereby avoiding the influence of boundary effects on the calculation results. Figure 4 shows the schematic diagram of artificial boundaries.

4. EXPERIMENTAL RESULTS AND ANALYSIS

Table 1 shows the variations in the comprehensive thermal conductivity of geomaterials, the comprehensive total thermal resistance of the buried pipe well, and the comprehensive heat capacity of geomaterials at different testing times. As the testing time increases, the comprehensive thermal conductivity of geomaterials gradually increases, rising from 2.47 W/(m·K) at 10 hours to 2.89 W/(m·K) at 20 hours, then fluctuating slightly, and finally returning to 2.89 W/(m·K) at 39 hours. The comprehensive total thermal resistance of the buried pipe well remains basically stable at different testing times, fluctuating between 0.051 and 0.061 m·K/W. The comprehensive heat capacity of geomaterials reaches a maximum value of 1.93 MJ/m³·K at 20 hours of testing time, then decreases slightly and stabilizes between 1.83 and 1.96 MJ/m³·K. The standard deviation gradually increases with the extension of testing time, indicating that the data dispersion

increases after prolonging the testing time, while the coefficient of determination remains consistently between 0.996 and 0.998, showing a high fitting accuracy.

The analysis of the experimental results shows that testing time has a certain impact on the thermal parameters of geomaterials. The comprehensive thermal conductivity of geomaterials gradually increases during the first 20 hours of testing time, indicating that the thermal conductivity improves as time extends during this stage. However, after exceeding 20 hours, the thermal conductivity tends to stabilize, indicating that the thermal conductivity of geomaterials approaches its saturation state during long-term testing. The comprehensive total thermal resistance of the buried pipe well remains basically stable, indicating that the thermal resistance characteristics of the system are not easily affected by testing time. The comprehensive heat capacity of geomaterials reaches its peak around 20 hours of testing time, then fluctuates slightly, but with a small range of variation. Although the standard deviation increases with time, the overall coefficient of determination remains at a high level, indicating good reliability of the test data. In summary, the test results indicate that within the testing time range of 20 hours, relatively stable and reliable thermal parameters of geomaterials can be obtained, providing important reference data for the thermal dynamic model of geomaterials in seismic engineering.

By analyzing the thermal stress-strain curve data of geomaterial samples at different temperatures (40°C, 30°C, 20°C) in Figure 5, it can be observed that as the temperature increases, the strain of the samples generally increases under the same axial stress. For example, when the axial stress reaches 100 MPa, the strain value at 40°C is 145, while at 30°C and 20°C, the values are 140 and 70, respectively, showing a significant temperature effect. Particularly in the high-stress region (e.g., above 300 MPa), the strain increases at 40°C is significantly larger, with the strain value reaching 380 at maximum stress, whereas the corresponding strain values at 30°C and 20°C are 447 and 290, respectively, indicating that the impact of high temperature on the thermal stress-strain of geomaterials is more pronounced. From the above experimental results, the following conclusion can be drawn: Temperature has a significant impact on the thermal stress-strain behavior of geomaterials, with higher temperatures leading to greater strain under the same stress, especially under high-stress conditions. This phenomenon can be attributed to the change in the mechanical properties of geomaterials at high temperatures, such as the decrease in elastic modulus and the loosening of internal structure, resulting in a reduced ability to resist deformation.

From the data of the relationship curves between the strength ratio and confining pressure of geomaterial samples at different temperatures in Figure 6, it can be seen that as the confining pressure increases, the strength ratio of the samples shows a decreasing trend. At 40°C, the strength ratio of the samples gradually decreases from 1.32 without confining pressure to 1.04 at 400 MPa confining pressure. At 30°C, the strength ratio decreases from 1.54 to 1.15. This indicates that, whether at a higher temperature of 40°C or a lower temperature of 30°C, the strength ratio of geomaterial samples decreases with the increase in confining pressure. Additionally, it can be observed that under the same confining pressure conditions, the strength ratio at 30°C is significantly higher than at 40°C. For example, at a confining pressure of 200 MPa, the strength ratio is 1.38 at 30°C, while it is only 1.16 at 40°C.

Based on the experimental results, the following conclusion is drawn: Confining pressure has a significant impact on the strength ratio of geomaterial samples, with the strength ratio gradually decreasing as the confining pressure increases. This phenomenon can be explained by the compression of internal pores in geomaterials under high confining pressure, leading to an increase in pore water pressure and a relative reduction in the overall strength of the geomaterials. Furthermore, the comparison at different temperatures shows that temperature has a significant effect on the strength ratio, with samples exhibiting higher strength ratios at lower temperatures (30°C), indicating that an increase in temperature further weakens the strength of geomaterials under high confining pressure conditions.
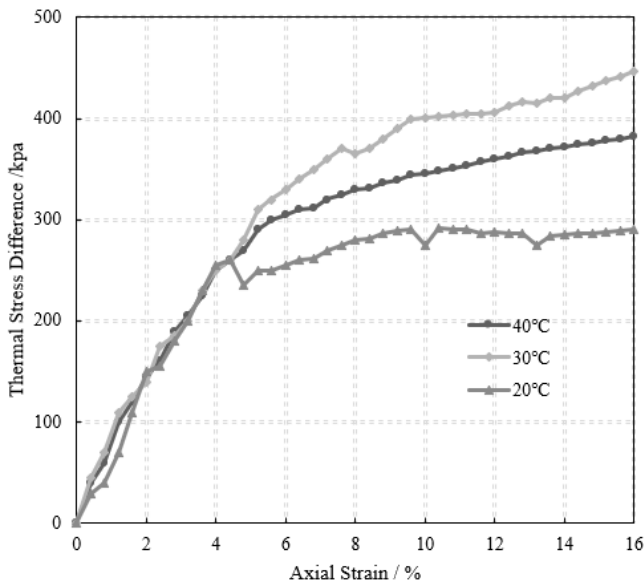

Figure 5. Thermal stress-strain curves of geomaterial samples at different temperatures
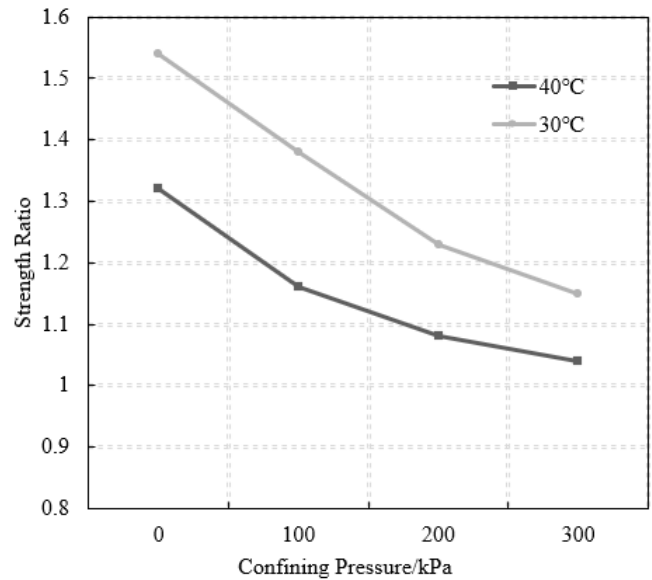

Figure 6. Relationship curves between strength ratio and confining pressure of geomaterial samples

Table 1. Analysis results at different testing times

Testing Time	Comprehensive Thermal Conductivity of Geomaterials	Comprehensive Total Thermal Resistance of Buried Pipe Well	Comprehensive Heat Capacity of Geomaterials	Standard Deviation	Coefficient of Determination
10 hours	2.47	0.051	1.78	0.086	0.998
15 hours	2.62	0.052	1.72	0.165	0.997
20 hours	2.89	0.061	1.93	0.213	0.997
25 hours	2.85	0.058	1.88	0.265	0.996
30 hours	2.78	0.057	1.87	0.223	0.996
35 hours	2.75	0.054	1.83	0.228	0.997
39 hours	2.89	0.057	1.96	0.234	0.996

Table 2. Comparison of experimental results and numerical simulations of peak horizontal acceleration at various measurement points in geomaterials for seismic engineering

	Measurement Point	1-5	1-10	1-15	1-20	1-25	1-30	1-35	1-40
0.1g	Experimental Value	0.098	0.121	0.182	0.235	0.275	0.132	0.184	0.256
	Simulation Value	0.132	0.201	0.245	0.356	0.421	0.189	0.256	0.345
0.2g	Experimental Value	0.212	0.225	0.321	0.487	0.589	0.263	0.374	0.526
	Simulation Value	0.265	0.421	0.478	0.648	0.745	0.389	0.548	0.635
0.4g	Experimental Value	0.452	0.456	0.625	0.924	1.235	0.489	0.765	0.989
	Simulation Value	0.538	0.723	0.945	1.232	1.326	0.724	1.125	1.237
0.6g	Experimental Value	0.685	0.662	0.912	1.065	1.678	0.721	0.932	1.158
	Simulation Value	0.789	0.945	1.265	1.689	1.923	0.987	1.389	1.623
0.8g	Experimental Value	0.889	0.856	1.178	1.206	1.987	1.056	1.003	1.458
	Simulation Value	1.121	1.425	1.685	2.126	2.234	1.189	1.568	2.236
1g	Experimental Value	0.987	1.185	1.364	1.452	2.189	1.268	1.189	1.523
	Simulation Value	1.324	1.874	1.925	2.236	2.874	1.562	2.014	2.236

Table 2 compares the experimental results and numerical simulations of peak horizontal acceleration at various measurement points in geomaterials under different seismic acceleration amplitudes. Overall, as the seismic acceleration amplitude gradually increases from 0.1g to 1g, both experimental values and simulation values exhibit an increasing trend. For example, at an acceleration of 0.1g, the experimental value at measurement point 1-25 is 0.275, while

the simulation value is 0.421; at an acceleration of 1g, the experimental value at measurement point 1-25 increases to 2.189, while the simulation value rises to 2.874. It can be seen that the numerical simulation values are generally higher than the experimental values, especially at higher acceleration amplitudes (e.g., 0.8g and 1g), where the differences are more pronounced. For measurement point 1-20, the experimental value is 0.235 at an acceleration of 0.1g, while the simulation value is 0.356; however, at an acceleration of 1g, the experimental value is 1.452, while the simulation value is as high as 2.236, showing a clear discrepancy. Based on the experimental results, the following conclusion can be drawn: the numerical simulation values are generally higher than the actual measured experimental values, particularly at higher seismic accelerations, where this difference becomes more significant. This may be because, during the numerical simulation process, the simplification of the model or the setting of boundary conditions may not fully reflect the actual situation of the samples, leading to higher simulation results under high-stress, high-acceleration conditions. Nevertheless, the overall trend of the simulation results and experimental results is consistent, indicating that the established model can to some extent accurately predict the dynamic response behavior of geomaterials under seismic action.
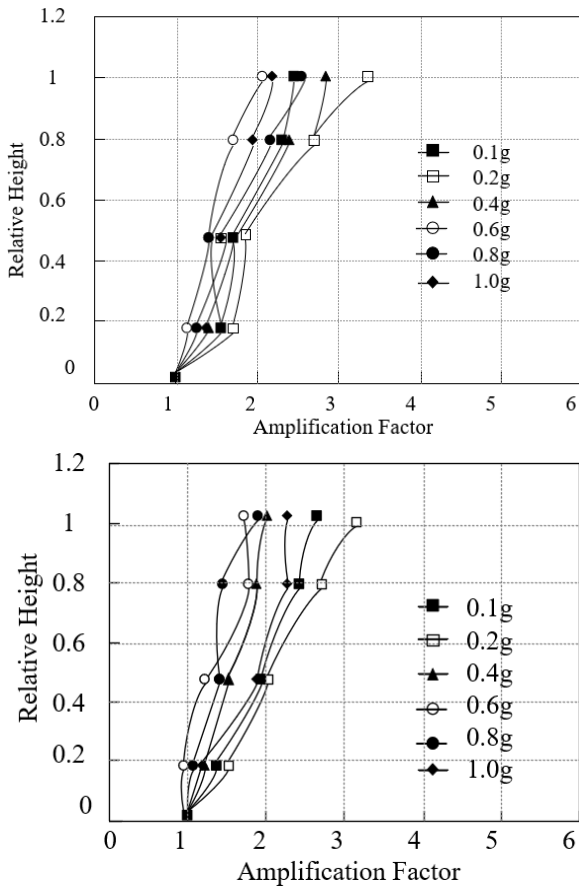
measurement points in geomaterials for seismic engineering. The results show that under the input of seismic horizontal acceleration, geomaterials exhibit a clear amplification effect, with numerical simulations showing that the amplification factor stabilizes at around 1.35, indicating that the geomaterials are in an elastic state under these conditions. Compared to the experimental test results, the peak horizontal acceleration values obtained from numerical simulations are generally higher, especially at higher acceleration amplitudes. This deviation is mainly attributed to the differences in the peak horizontal acceleration of the concrete bedrock, as well as potential errors that may arise during the testing apparatus setup and vibration table loading process. For example, at higher acceleration amplitudes, the amplification factors shown by the experimental results are slightly lower than the simulation results, indicating that the actual response of geomaterials may be slightly weaker than that predicted by the numerical model. Despite the differences in horizontal acceleration amplification factors between the numerical simulation results and actual experimental results, the overall trends are consistent, and the numerical simulation results can generally reflect the dynamic response characteristics of geomaterials under seismic action. These differences may stem from the installation and loading errors in the model test that are difficult to completely avoid but do not significantly affect the overall judgment of geomaterial behavior.
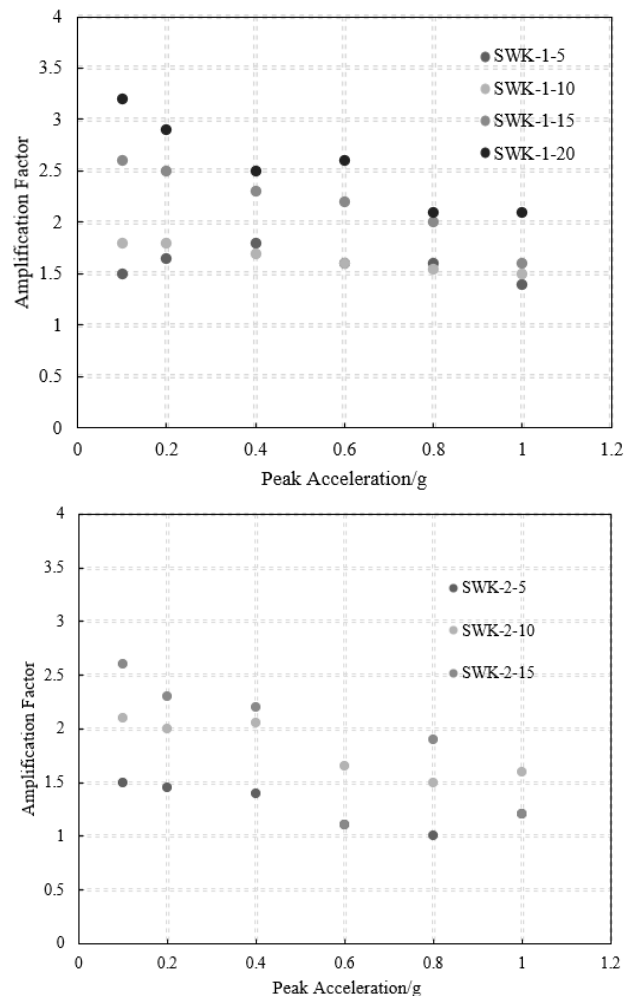

Figure 7. Distribution of horizontal acceleration amplification factors in geomaterials for seismic engineering

In the experiment on geomaterials in seismic engineering, Figure 7 shows the comparison between the experimental test results and numerical simulation results of the distribution of horizontal acceleration amplification factors. Figure 8 provides the relationship between the horizontal acceleration amplification factors and the peak acceleration at various

Figure 8. Relationship between horizontal acceleration amplification factor and peak acceleration at various measurement points in geomaterials for seismic engineering

Table 3. Fitting parameters for the relationship between acceleration amplification factor and seismic intensity at different compaction levels in geomaterials for seismic engineering

Compaction Level		Geomaterial Surface Measurement Points			Geomaterial Section Measurement Points	
		2-10	2-15	2-20	2-25	2-30
95%	Experimental Value	1.265	1.356	2.189	1.203	1.568
	Simulation Value	-0.234	-0.521	-0.325	-0.326	-0.487
91%	Experimental Value	1.128	1.326	1.892	1.225	1.456
	Simulation Value	-0.175	-0.452	-0.389	-0.278	-0.356
87%	Experimental Value	1.326	1.326	2.315	1.478	1.536
	Simulation Value	-0.024	-0.365	-0.189	-0.045	-0.485
83%	Experimental Value	1.235	1.326	1.658	1.289	1.007
	Simulation Value	-0.038	-0.198	-0.512	-0.135	-0.732

In this experiment, by analyzing the response of geomaterials to the input seismic acceleration in seismic engineering, it was found that geomaterials exhibit a significant amplification effect on acceleration, and this amplification effect increases with the depth of the geomaterials. Specifically, as the peak acceleration of seismic excitation increases, the horizontal acceleration amplification factor shows a decreasing trend. This phenomenon indicates that as the excitation intensity increases, the shear strain and damping ratio within the soil increase, and the geomaterials gradually exhibit nonlinear characteristics, leading to an enhanced filtering effect. The experimental results show that the range of horizontal acceleration amplification factors for geomaterials in seismic engineering is between 1 and 3.15, while the horizontal acceleration amplification factors of geomaterial sections range from 1 to 3.26. Consistent with the conclusions of the vibration table test, these data further verify the dynamic response characteristics of geomaterials at different depths and excitation intensities.

Comprehensive analysis of the experimental results leads to the conclusion that the acceleration amplification effect of geomaterials under seismic action is significant, and the amplification factor is greatly influenced by the intensity of seismic excitation and the depth of the soil. When the seismic excitation intensity is relatively low, the geomaterials exhibit relatively large amplification factors, but as the excitation intensity increases, the amplification factors gradually decrease, mainly due to the enhanced nonlinear characteristics within the geomaterials. Additionally, the experimental results are consistent with the conclusions of the vibration table test, further confirming the stress-strain evolution laws of geomaterials under different depths and excitation conditions.

Table 3 shows the relationship between the acceleration amplification factor and seismic intensity in geomaterials for seismic engineering under different compaction conditions, comparing experimental values and simulation values. At compaction levels of 95%, 91%, 87%, and 83%, the experimental values at various measurement points show that the acceleration amplification factor of geomaterials fluctuates with the decrease in compaction. For example, at measurement point 2-20, the experimental value is 2.189 at 95% compaction, while at 87% compaction, it increases to 2.315. It is noteworthy that there is a significant difference between the simulation values and experimental values, with simulation values generally being negative and showing little variation with the decrease in compaction. For instance, at measurement point 2-20, the simulation value changes from -0.325 (95% compaction) to -0.189 (87% compaction). This negative simulation result significantly deviates from the experimental values, particularly under high compaction conditions, where the difference between simulation results and actual experimental results is most pronounced. The analysis of the experimental results indicates that compaction has a significant impact on the acceleration amplification factor of geomaterials. The experimental results show that as compaction decreases, there is some fluctuation in the acceleration amplification factor of geomaterials, demonstrating the nonlinear response characteristics of geomaterials under seismic action. However, there is a significant difference between the numerical simulation results and experimental results, especially under high compaction conditions, where the simulation values exhibit unreasonable negative values. This discrepancy may be due to the fact that the model settings during the simulation process failed to accurately reflect the physical properties and stress conditions of the actual geomaterials, or due to improper handling of the geomaterials' response under dynamic loading in the numerical simulation method.

5. CONCLUSION

This study conducted an in-depth analysis and discussion on the dynamic thermal response of geomaterials in seismic engineering. First, a reasonable heat transfer model was selected and established to provide a theoretical basis for simulating the behavior of geomaterials under the combined action of thermal stress and dynamic loads. By analyzing the comprehensive thermal conductivity, comprehensive total thermal resistance of the buried pipe well, and comprehensive heat capacity of geomaterials at different testing times, the impact of testing time on the thermal parameters of geomaterials was revealed, indicating that stable and reliable parameters can be obtained within 20 hours. Additionally, the study delved into the stress-strain evolution laws of geomaterials under the coupling effects of temperature and dynamic loads, and combined experimental results such as thermal stress-strain curves, strength ratio, and confining pressure relationships to analyze the mechanical properties of geomaterials and their response to seismic motions. The study also conducted a fitting analysis of the relationship between the acceleration amplification factor and seismic intensity in geomaterials for seismic engineering under different compaction levels, verifying the model's effectiveness and comparing experimental results with numerical simulation results, further deepening the understanding of the nonlinear response characteristics of geomaterials.

This study holds important value in both theoretical and practical applications. The heat transfer model established and the systematic analysis of the dynamic thermal response of geomaterials provide strong support for accurately simulating the behavior of geomaterials in seismic engineering, which is

of great significance for improving the reliability of seismic engineering design. Furthermore, by thoroughly analyzing the dynamic characteristics of geomaterials under different compaction and temperature conditions, this study offers new perspectives and methods for predicting and designing geomaterial behavior in engineering applications. Despite the many meaningful results obtained, there are still certain limitations in this study. First, there remain some differences between the numerical simulation and experimental results, especially under high compaction conditions, which may be due to the limitations of model assumptions and parameter settings. Second, this study mainly focused on the thermal-dynamic coupling response of geomaterials, without delving into the effects of other environmental factors such as humidity changes and chemical actions on geomaterial behavior.

Future research can be expanded in the following areas: first, optimizing and improving existing heat transfer models and numerical simulation methods to further narrow the gap between simulation results and experimental data; second, expanding the range of environmental factors studied to explore the mechanical behavior of geomaterials under multi-factor coupling conditions such as humidity and chemical actions; third, conducting larger-scale experimental studies to verify the applicability of the model under different engineering conditions, thereby enhancing the engineering application value of the research findings. These further studies will contribute to a more comprehensive understanding and prediction of the complex behavior of geomaterials in seismic engineering, providing more precise guidance for engineering design.

REFERENCES

[1] Rieksts, K., Eberg, E. (2022). Experimental study on the effect of soil moisture content on critical temperature rise for typical cable backfill materials. IEEE Transactions on Power Delivery, 38(3): 1636-1648. https://doi.org/10.1109/TPWRD.2022.3220954

[2] Liu, J., Zhang, Y., Wang, Z., Zhou, C., Liu, B., Wang, F. (2023). Medium rock-soil temperature distribution characteristics at different time scales and new layout forms in the application of medium-deep borehole heat exchangers. Energies, 16(19): 6970. https://doi.org/10.3390/en16196970

[3] Krishnaiah, S., Singh, D.N., Jadhav, G.N. (2004). A methodology for determining thermal properties of rocks. International Journal of Rock Mechanics and Mining Sciences, 41(5): 877-882. https://doi.org/10.1016/j.ijrmms.2004.02.004

[4] Zhang, Y., Hao, S., Yu, Z., Fang, J., Zhang, J., Yu, X. (2018). Comparison of test methods for shallow layered rock thermal conductivity between in situ distributed thermal response tests and laboratory test based on drilling in northeast China. Energy and Buildings, 173: 634-648. https://doi.org/10.1016/j.enbuild.2018.06.009

[5] Huang, S., Li, J., Zhu, K., Dong, J., Jiang, Y. (2023). Thermal recovery characteristics of rock and soil around medium and deep U-type borehole heat exchanger. Applied Thermal Engineering, 224: 120071. https://doi.org/10.1016/j.applthermaleng.2023.120071

[6] Jemmal, Y., Zari, N., Maaroufi, M. (2016). Thermophysical and chemical analysis of gneiss rock as low cost candidate material for thermal energy storage in concentrated solar power plants. Solar Energy Materials and Solar Cells, 157: 377-382. https://doi.org/10.1016/j.solmat.2016.06.002

[7] Allen, K.G., Von Backström, T.W., Kröger, D.G., Kisters, A.F.M. (2014). Rock bed storage for solar thermal power plants: Rock characteristics, suitability, and availability. Solar Energy Materials and Solar Cells, 126: 170-183. https://doi.org/10.1016/j.solmat.2014.03.030

[8] Huang, Y., Zhang, Y., Gao, X., Ma, Y. (2022). Thermal disturbance analysis in rock-soil induced by heat extraction from the abandoned well. Geothermics, 101: 102374. https://doi.org/10.1016/j.geothermics.2022.102374

[9] Jia, G.S., Tao, Z.Y., Meng, X.Z., Zhang, L.Y., Chai, J.C., Jin, L.W. (2019). A new analytical model for the estimation of three-phase rock-soil thermal conductivity for geothermal utilization. In IOP Conference Series: Earth and Environmental Science, 268(1): 012001. https://doi.org/10.1088/1755-1315/268/1/012001

[10] Laubscher, H.F., von Backström, T.W., Dinter, F. (2017). Developing a cost effective rock bed thermal energy storage system: Design and modelling. In AIP Conference Proceedings, 1850(1). https://doi.org/10.1063/1.4984436

[11] Santander, R.E., Bubnovich, V. (2002). Assessment of mass and heat transfer mechanisms in unsaturated soil. International Communications in Heat and Mass Transfer, 29(4): 531-545. https://doi.org/10.1016/S0735-1933(02)00350-0

[12] Gune, M., Harshavardhana, B.G., Balakrishna, K., Udayashankar, H.N., Shankar, R., Manjunatha, B.R. (2016). Rock magnetic finger-printing of soil from a coal-fired thermal power plant. Environmental Monitoring and Assessment, 188(5): 1-13. https://doi.org/10.1007/s10661-016-5279-2

[13] Shibahara, Y., Kubota, T., Fujii, T., Fukutani, S., Takamiya, K., Konno, M., Mizuno, S., Yamana, H. (2016). Determination of isotopic ratios of plutonium and uranium in soil samples by thermal ionization mass spectrometry. Journal of Radioanalytical and Nuclear Chemistry, 307(3): 2281-2287. https://doi.org/10.1007/s10967-015-4551-1

[14] Sauer, D., Wagner, S., Popov, Y., Rose, F., Schramm, A., Börner, E., Wünsch, T., Redondo-Robles, H., Hesse, G., Pfeiffer, J. (2017). Development of a new borehole probe for thermal conductivity scanning. Geothermics, 67: 95-101. https://doi.org/10.1016/j.geothermics.2017.02.003

[15] Milun, S., Kilic, T., Bego, O. (2005). Measurement of soil thermal properties by spherical probe. IEEE Transactions on Instrumentation and Measurement, 54(3): 1219-1226. https://doi.org/10.1109/TIM.2005.847223

[16] Chauchois, A., Antczak, E., Defer, D., Brachelet, F. (2012). In situ characterization of thermophysical soil properties—Measurements and monitoring of soil water content with a thermal probe. Journal of Renewable and Sustainable Energy, 4(4). https://doi.org/10.1063/1.4737138

[17] Li, B., Ju, F. (2018). Thermal stability of granite for high temperature thermal energy storage in concentrating solar power plants. Applied Thermal Engineering, 138: 409-416. https://doi.org/10.1016/j.applthermaleng.2018.04.071

[18] Dehghani, B., Amirkiyaei, V., Ebrahimi, R., Ahmadi, H., Mohammadzamani, D., Zavareh, S.B. (2020). Thermal loading effect on P-wave form and power spectral density in crystalline and non-crystalline rocks. Arabian Journal of Geosciences, 13(16): 1-9. https://doi.org/10.1007/s12517-020-05779-9

[19] Zheng, Y.X, Zhang, T.J, Yang, H.T, Wang, W., Niu, Q.H, Wei, H.Y. (2023). An experimental investigation on mechanical properties and failure characteristics of layered rock mass. Applied Sciences, 13(13): 7537. https://doi.org/10.3390/app13137537

[20] Srivastava, L.P. (2022). Analysis of a rock bolt-reinforced tunnel with equivalent mechanical properties. Indian Geotechnical Journal, 52(4): 815-834. https://doi.org/10.1007/s40098-022-00631-1